Characterization of sugarcane leaf-biomass and investigation of its efficiency in removing Nickel(II), Chromium(III) and Cobalt(II) ions from polluted water

Oludoyin Adeseun Adigun[a,1*], Vincent Olukayode Oninla[b*], N. A. Adesola Babarinde[c], K.O. Oyedotun[d], Ncholu Manyala[d].

a. Department of Chemistry, University of Ibadan, Ibadan, Nigeria.
b. Department of Chemistry, Obafemi Awolowo University, Ile-Ife, Nigeria.
c. Department of Chemical Sciences, Olabisi Onabanjo University, Ago-Iwoye, Nigeria.
d. Department of Physics, Institute of Applied Materials, Carbon Technology and Materials, University of Pretoria, Pretoria 0002, South Africa.

[1]Current Address: School of Science and the Environment/Boreal Ecosystem Research Facility, Grenfell Campus, Memorial University of Newfoundland, 20 University Drive, Corner Brook, NL A2H 5G4, Canada.

[*]*Corresponding Authors:* oaadigun@mun.ca (OAA), vinzoninla@daad-alumni.de (VOO); +1-709-770-3747, +234(0)-706-537-7096

Highlights

• All the major components of the biomass participated in the metal ions removal.

• Adsorption of the metal ions resulted in surface folding.

• Pseudo-second-order model best explain the kinetic of the adsorption processes.

• Adsorption of Ni^{2+}, Cr^{3+} and Co^{2+} ions occurred at specific homogeneous sites.

• The metal removal processes were physical in nature.

Abstract

Sugarcane leaves biomass (SCL) has been utilized for the removal of Ni^{2+}, Cr^{3+} and Co^{2+} ions from polluted water. Qualitative analysis was performed by Fourier Transformed Infra-Red spectroscopy, Raman spectroscopy, scanning electron microscopy coupled with energy dispersive spectroscopy and X-ray diffractometry. Adsorption of the metal-ions was carried out by contacting 50 mL of known concentration of Ni^{2+}, Cr^{3+} and Co^{2+} with known amount of SCL at 27 ºC, and under varied experimental conditions such as pH, ionic strength, solid-to-liquid ratio, contact time and initial metal ions concentration in batch

adsorption experiment. The kinetics, isothermal, as well as the nature of the adsorption were predicted by models such as pseudo-first-order, pseudo-second order, Elovich, Weber-Morris, Freundlich, Langmuir, Temkin and Dubinin-Raduschevich. The thermodynamics of the processes was also predicted. Characterization analyses portrayed the surface of SCL as being porous, oval in shape and composed of hydroxyl and carbonyl groups as the main binding sites. Raman analysis revealed the interaction of the metal ions with the lignin, cellulose as well as hemicellulose components of the adsorbent. Adsorption of Ni^{2+} and Co^{2+} ions was favored by increasing pH, while that of Cr^{3+} ions was mostly favored at pH 4. Metal uptake increased with increasing contact time and concentration up to equilibrium stage. The sorption processes followed the pseudo-second-order kinetics and was monolayer in nature with q_{max} of 51.3, 62.5, and 66.7 mg/g for the uptake of Ni^{2+}, Cr^{3+} and Co^{2+} ions, respectively. The models predicted physisorption as the main process involved. Thermodynamic study showed that the processes were feasible and spontaneous, endothermic, and occurred with increase in randomness at the adsorbate-adsorbent interface, demonstrating a good metal uptake nature of the adsorbent.

Graphical abstract

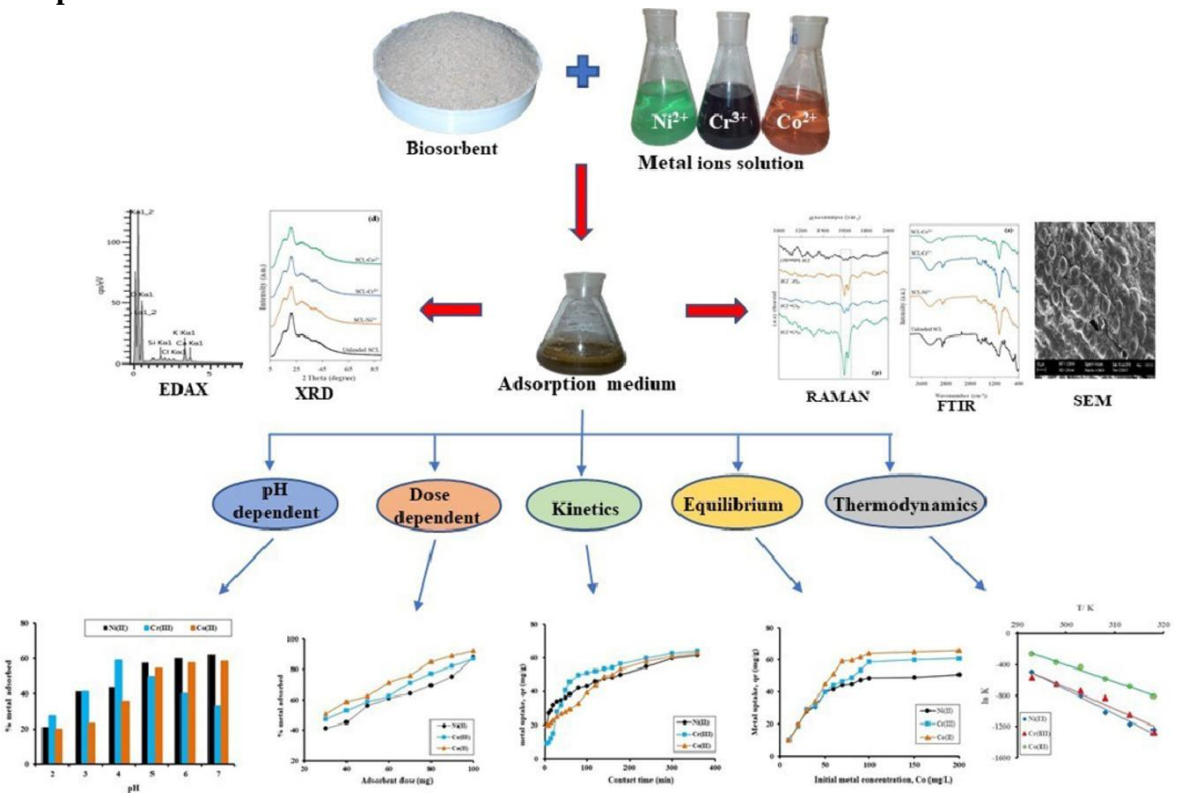

KEYWORDS: Adsorption, Sugarcane leaves, polluted water, Equilibrium, Monolayer, Physisorption

1 Introduction

Environmental pollution, especially that of water bodies, has become a major threat to human existence in life. Unfortunately, it has been on the increase due to rapid population growth and advancement in science and technology [1] without proper measures being put in place to check excesses, particularly in developing countries. Most of the effluents from the industries contain toxic compounds that are non-biodegradable [2]. Heavy metals such as mercury (Hg), cadmium (Cd), lead (Pb), nickel (Ni), zinc (Zn), chromium (Cr) and cobalt (Co) are released from metal processing industries, while various dyes are discharged from textile and dye industries [2,3]. Other compounds entering the water bodies, either from industries or other human practices, include agro-chemical residues and pharmaceutical drugs [4]. Many of these contaminants are very toxic at elevated concentrations and injurious to the ecosystem [5]. Most diseases such as various forms of cancer, renal failure or disorder, dermatitis, and respiratory hypersensitivity have been traced to ingestion of heavy metals and other toxic substances from water [6]. Due to their non-biodegradable nature, ingestion of this toxins by aquatic organisms results in bioaccumulation in the food chain, resulting in chronic illnesses and even death of aquatic organisms and humans [7].

Water is indispensable! Due to its great importance, water issue has constituted a great global challenge and it has attracted the attentions of numerous environmental experts and activists. Various regional blocs and countries have also constituted their regulatory bodies to preserve lives by regulating or preventing the abuse of the environment through misuse or mistreatment of water bodies. A surge in water pollution has been noticed among the underdeveloped and developing countries since the 1990s. This is expected to worsen in years to come, posing a great health risk to humans and threat to the environment [1]. Since the demand for clean water is on the increase, water remediation then becomes imperative.

Attempts have been and are still being made to combat the menace of water pollution. Methods employed in removing toxic substances or compounds from wastewater so far include chemical precipitation, chemical oxidation, ion exchange, coagulation and flocculation, electrochemical precipitation, membrane separation, aerobic and anaerobic degradation [8-10] and adsorption [11]. Though effective in some ways, many of these techniques have their own draw backs such as excessive use of chemicals, generation of secondary pollutants in form of sludge which are difficult to dispose. Most of the methods are capital intensive, making large scale water purification challenging, especially in underdeveloped and low-income countries [12]. Adsorption, on the other hand, appears very promising due to the advantages it has over other techniques. Water remediation by adsorption process is affordable and yet effective. Other superior advantages of this method include simplicity of design and operation, minimization of biological sludge, reusability of adsorbent, adsorbate recovery and availability of raw materials [3,13]. The method is based on mass transfer of contaminants from the bulk liquid phase to the

surface of an adsorbent which serves as solid phase. Over time, it has positioned itself as efficient alternative method for wastewater treatment [1].

Due to their carcinogenic and mutagenic effects, removal of heavy metals from wastewaters have attracted the attention of researchers in the field of adsorption, and the search for effective adsorbents has become a major point of attraction. Efficiencies of g-C_3N_4, a graphitic-like carbon nitride and g-C_3N_4-based materials, on the removal of toxic heavy metals in aqueous medium have been reported. These materials bind to pollutants by forming strong surface complexes [14,15]. Moreover, due to abundance of functional groups, variable porous structures and chemical stability, metal-organic frameworks (MOFs) have been utilized in the removal of radionuclides [16].

Based on natural material, several adsorbents of biological and agricultural origins have been investigated for their metal removal abilities and a number of them have shown promising prospects. Sari and Tuzen have reported the use of *Amanita rubescens* biomass in the removal of Pb(II) and Cd(II) from aqueous medium [17], while Oninla *et al*., have reported the removal of Cd^{2+}, Pb^{2+}, Ni^{2+} and Cr^{3+} by biomass of oil palm calyxes [7]. Other adsorbents whose metal removal abilities have been reported include castor seed hull [18], rice straw [19], sugar beet pulp [20] and *Undaria pinnatifida* [21]. The list keeps growing, with efforts being made at modifying the adsorbents for better performance.

The main aim of this study was to investigate the adsorptive efficiencies of SCL (a biomass prepared from sugarcane leaves) in the sequestration of Ni^{2+}, Cr^{3+} and Co^{2+} ions from aqueous medium. Earlier report had shown the effectiveness of the adsorbent in the removal of Cd^{2+}, Pb^{2+} and Zn^{2+} ions [22]. Several bio-adsorbents exhibit broad range metal binding while some show specific affinity for certain metals [23]. Most industrial wastewaters are composed of a mixture of different cations and pollutants. Understanding the performance of the adsorbent on the removal of a broad range heavy metal pollutants and their removal mechanism will give an insight into the possible efficiency of the biomass on a large-scale industrial application. Sugarcanes are cultivated in large scale in some tropical and subtropical countries, Nigeria being one of the countries whose climate support the growth of the plant. Economically, the point of attraction is the succulent part of the stem from which sugarcane juice is extracted, while other parts constitute agricultural wastes. Although animals often feed on the leaves, larger portions of the leaves are left as waste, especially in large-scale sugarcane plantations. Utilizing the agro-waste as adsorbent, therefore, will serve as an alternative use and a means of converting waste to wealth.

In this report, different physicochemical characterization technique such as Fourier Transform Infra-Red Spectroscopy (FTIR), Raman spectroscopy, Scanning Electron Microscopy (SEM) coupled with energy dispersive spectroscopy (EDAX), and X-ray diffractometry (XRD) were utilized in understanding the qualities of the SCL. The impact of different parameters such as solution pH, ionic strength, time, adsorbent dose and concentration were evaluated, and various optimal conditions established in

understanding the efficacy of the adsorbent. Moreover, attempt was made in gaining insight into the nature and mechanism of the meta ion removal process by investigating the thermodynamics of the process as well as fitting the adsorption data into various kinetic and isothermal models.

2 Material and methods

2.1 Preparation and characterization of sugarcane leaf-biomass

The sugarcane leaf-biomass (SCL) was prepared as earlier described [22]. Briefly, sugarcane leaves were sourced from a sugarcane plantation located at Mamu village in Ijebu-Igbo, Ogun State, Nigeria. The agro-waste was surface rinsed with tap and deionized water to remove any adhering impurities. The washed leaves were air-dried for 14 days and then dried at 70^{o}C for 5 h, followed by grinding and sieving to $\leq$ 450 μm particle sizes. The sieved portion, subsequently called SCL, was oven dried to constant weight at 50 ^{o}C, and then kept in an air-tight plastic container for later use. Qualitative analysis of the adsorbent (raw (unloaded) and metal loaded samples), were performed by Fourier Transform Infra-Red Spectroscopy (FTIR), Raman spectroscopy, Scanning Electron Microscopy (SEM) coupled with energy dispersive spectroscopy (EDAX), and X-ray diffractometry (XRD).

2.2 Preparation of adsorbate solution

The adsorbates used in this study were nickel(II), chromium(III) and cobalt(II) ions, prepared from their metal salts – $NiSO_4.6H_2O$, $Cr(NO_3)_3.9H_2O$ and $CoSO_4.7H_2O$ which were purchased from Sigma-Aldrich. To prepare metal ion solutions, accurately weighed amount of the respective metal salts were dissolved in deionized water in a 1 L standard volumetric flask and then made up to the mark. Appropriate working solutions were prepared from the stock solutions by serial dilution. To further confirm the concentration prepared, the metal solutions were standardized using Atomic Absorption Spectrophotometer (Buck-Scientific 210 VGP) with deuterium background correlator.

2.3 Adsorbate removal process

The process of removal of the adsorbates (metal ions) from solutions containing them was carried out by batch adsorption study. Parameters whose effects on the removal process were studied include pH, ionic strength, contact time, solid-to-liquid ratio (dose dependent) and initial metal-ion concentration. The isothermal behaviour, kinetics and thermodynamics of the removal process were also investigated. Figure 1 shows a scheme summarizing the major steps involved in this research. All studies were undertaken in, at least, duplicate. The chosen adsorbent mass for this study (excluding dose dependent study) was 50 mg. With the exception of the effect of initial metal-ion solution, 50 mg SCL was contacted with 100 mg/L metal-ion (Ni^{2+}, Cr^{3+}, Co^{2+} ions) solution in corked 250 mL Erlenmeyer flasks and allowed to equilibrate

for 2 h (excluding effect of contact time) at 200 rpm in a thermostatic water bath with shaker (Haake Wia model, Germany). The studies (excluding thermodynamic study) were allowed to proceed at room temperature, which was at around 27°C. The pH dependent study was performed from pH 2 to 7. Solution pH was adjusted by dropwise addition of either HNO_3 or NaOH. Effect of ionic strength was performed at the optimum pH for individual metal ion with NaCl as background electrolyte. NaCl concentration was varied from 0.001 to 0.1 M. Time dependent study was performed by varying the agitation time from 0 – 360 min; dose dependent study was performed by varying adsorbent mass from 30 – 100 mg; initial metal-ion concentration was varied from 10 – 200 mg/L; while thermodynamic study was performed at temperature range of 20 – 45 ºC. Samples were withdrawn from the shaker and filtered using Whatman's #42 filter papers. Analysis of the filtrates for residual metal ions was performed using atomic absorption spectrophotometer. Metal-ion uptake and percentage metal-ion uptake by SCL were subsequently determined according to equation 1 and 2.

$$\% \text{ adsorbed} = \frac{(C_o - C_e)}{C_o} \times 100 \quad \text{.....1}$$

$$q_e = \frac{(C_o - C_e)V}{m} \quad \text{.....2}$$

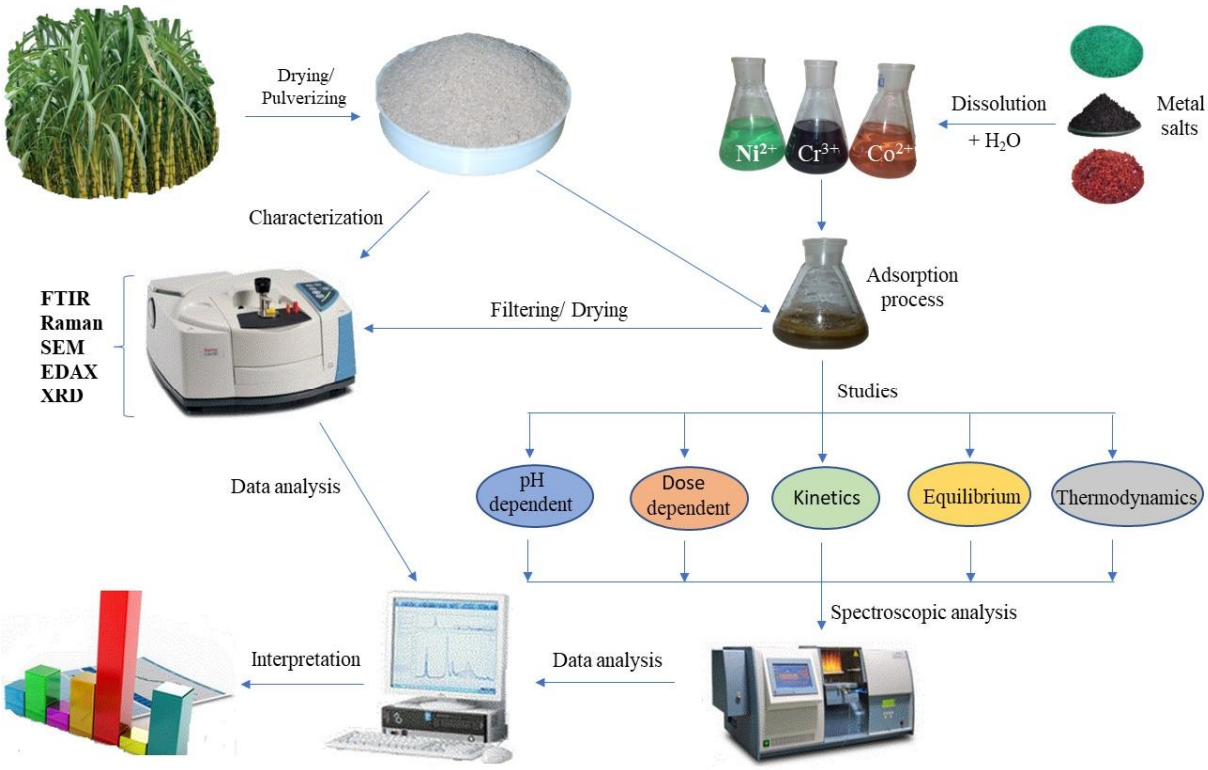

Fig. 1 Highlight of the major steps in the adsorption of Ni^{2+}, Cr^{3+} and Co^{2+} by SCL

Where C_o and C_e stand for initial and equilibrium adsorbate concentration in mg/L, m (g) stands for SCL mass, and V (L) stands for solution volume.

In order to determine the kinetics of the process and the best isotherms that describe the experimental data, models such as Lagergren pseudo-first order [24], pseudo-second order [25], Elovich [26], Weber-Morris Intraparticle Diffusion [27]), Langmuir [28], Freundlich [29], Temkin [30] and Dubinin-Radushkevich were applied to the experimental data. The linear equation for the above listed kinetics and equilibrium models are represented by equations 3 to 10.

Lagergren Pseudo-first order: $\ln (q_e - q_t) = \ln q_e - k_1 t$ ……3

Pseudo second order: $\frac{t}{q_t} = \frac{t}{q_e} - \frac{1}{k_2 {q_e}^2}$ …… 4

Elovich: $q_t = \frac{1}{\beta}\ln[\alpha\beta] + \frac{1}{\beta}\ln t$ ……5

Weber–Morris: $q_t = k_\alpha t^{½} + C$ ……6

Langmuir: $\frac{C_e}{q_e} = \frac{1}{q_{max} K_L} + \frac{C_e}{q_{max}}$ …… 7

Freundlich: $\ln q_e = \ln k_f + \frac{1}{n}\ln C_e$ …… 8

Temkin: $q_e = B\ln A_T + B\ln C_e$ …… 9

Dubinin-Radushkevich: $\ln q_e = \ln q_m - \beta\varepsilon^2$ ……10

Where: $\varepsilon = RT\, ln\left(1 + \frac{1}{C_e}\right)$ (J/mol), which denotes Polanyi potential; q_e and C_e are as earlier defined; q_t (mg/g) denotes adsorbate uptake at time *t*; k_1 (min^{-1}), k_2 (g/mg min) and k_α (mg/g $min^{½}$) denote the rate constants for the pseudo-first-order, pseudo-second-order and intra-particle diffusion models, respectively; *C* denotes intercept; q_{max} (mg/g), K_L (L/mg), K_f (mg/g) and n denote maximum adsorption capacity, Langmuir constant, Freundlich constant and intensity constant, respectively; *R* (8.314 J/mol K) denotes gas constant; while *T* (K) and β (mol^2/kJ^2) denote temperature and D–R constant, respectively; B = RT/b represents Temkin constant; A_T (L/g) is Temkin adsorption potential; α is the initial rate of adsorption (mg/g.min), and β represents desorption constant in Elovich. Required parameters (from the models applied) were obtained from the slopes and intercepts of the linear plots of the integral equations of the models. These parameters were interpreted to determine the models that suitably described the adsorption process.

3 Results and Discussion

3.1 Qualitative analysis of the biomass

3.1.1 FT-IR and Raman analyses of SCL

The functional groups active at the surface of an adsorbent play a pivotal role in adsorbate removal. To determine the active functional groups at the SCL's surface, FTIR analysis of the unloaded and metal-ion loaded samples were performed by FTIR - spectrum version 2, (PerkinElmer), at the scanning frequencies of 400 – 4000 cm^{-1}. As shown in Figure 2a, the spectrum of the unloaded sample revealed a number of absorption peaks, prominent among which are those of the O–H/N–H stretching vibration at 3333 cm^{-1} [12], symmetric and asymmetric C–H stretch at 2918 and 2850 cm^{-1}), ester C=O group and aromatic C=O stretch at 1733 and 1635 cm^{-1}, lignin C-O linkage at 1507 cm^{-1} [22], C–O–C vibration in cellulose and hemicellulose at 1158 cm^{-1}, and C–O bending at 1035 cm^{-1} [31]. The spectra obtained after adsorption of Ni^{2+}, Cr^{3+} and Co^{2+} ions suggest strong interactions of the metal ions with the hydroxyl and carboxyl functional groups on the surface of SCL. This is indicated by the significant shift in the –OH and C=O bands after metal uptake as shown in Table 1. Alterations in absorption peaks were also observed in the bands ascribed to C-O of lignin linkage, C–O bending as well as C–H deformation in cellulose and hemicellulose, suggesting the contribution of lignin, cellulose, as well as hemicellulose parts of the adsorbent in the adsorption process.

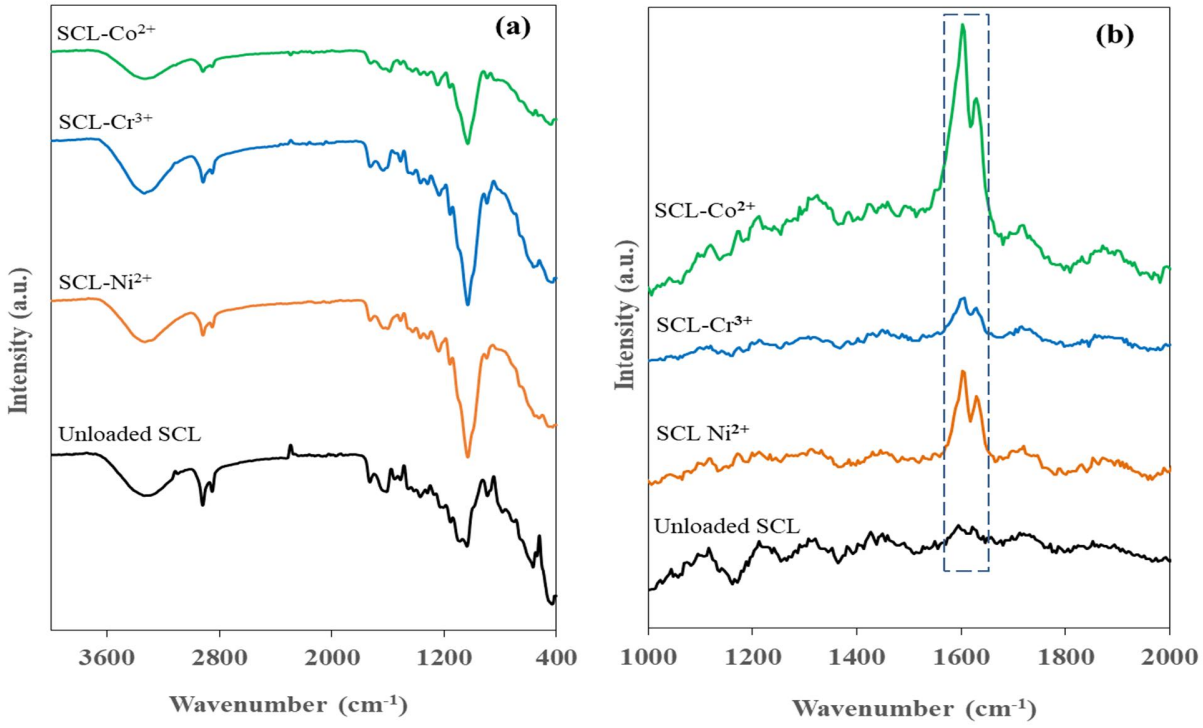

Fig. 2 FTIR and Raman spectra of unloaded and metal-loaded SCL

Table 1 FTIR and Raman bands observed in SCL and their assignment. (Band intensities – *vs*: very strong, *s*: strong, *m*: medium, *w*: weak, *sh*: shoulder)

FTIR					**RAMAN**				
Assignment	***Peak Position (cm^{-1})***				***Assignment***	***Peak Position (cm^{-1})***			
	RAW	**Ni^{2+}**	**Cr^{3+}**	**Co^{2+}**		**RAW**	**Ni^{2+}**	**Cr^{3+}**	**Co^{2+}**
O-H/N-H str	3333	3325	3335	3335	*Ring conjugated C=C str. of lignin* [32,34]	1629_{m}	1633_{vs}	1633_{s}	1633_{vs}
C-H, sym	2918	2917	2917	2915	*Ring conjugated C=C str. of lignin*	1605_{m}	1605_{vs}	1605_{s}	1605_{vs}
C-H, asym	2850	2849	2849	-	*Aryl ring sym. Str. in lignin* [32,35]	-	-	1597_{sh}	-
Ester C=O grp	1733	1727	1727	1737	*OCH_3 deformation; CH_3 bend + ring str. of lignin* [32,34]	1429_{m}	1434_{w}	1431_{w}	1433_{m}
Aromatic str C=O	1635	1603	1632	1635	*HCC, HCO, and HOC bending in cellulose and hemicellulose* [35]	1389_{m}	1389_{w}	1389_{w}	1389_{m}
lignin, C–O linkage	1507	1513	1513	1505		1323_{w}	1333_{w}	-	1327_{m}
C–H deformation in cellulose and hemicellulose	1373	1369	1367	1373	*Aryl-O of aryl-OH and Aryl-OCH_3; C=O group of guaiacyl* [32]	1224_{m}	1222_{w}	1224_{w}	1218_{m}
	1269	1239	1234	1237	*COC sym. Str. in cellulose/hemicellulose* [35]	1121_{m}	1124_{w}	1124_{w}	1124_{m}
C–O–C vibration in cellulose and hemicellulose	1158	1159	1159	1156	*COC asym. Str. in cellulose/hemicellulose* [35]	1039_{m}	1040_{w}	-	1040_{m}
C-O bending	1035	1032	1032	1033					

The Raman spectra of the SCL samples were obtained by the use of a WITec Confocal Raman Microscope (WITec alpha 300 R, Germany), Laser wavelength 532 nm, laser power 4 mW and spectral acquisition time 120-s was used in order to identify the lignocellulose characteristic Raman peaks, as well as characterize the surface interaction between Ni^{2+}, Cr^{3+} and Co^{2+} ions and SCL. Raman spectroscopy methods are employed in the determination of the structural characteristics and the spread of chemical components in lignocellulosic materials [31]. Both electrically symmetrical and non-symmetrical bonds are completely revealed by these methods. The major components of plant biomass are the polysaccharides (mainly cellulose and hemicellulose) and lignin. These components exhibit characteristic Raman peaks.

Although hemicellulose displays similar Raman band as cellulose, its bands are usually shifted towards lower frequencies [32]. Lignin is often identified with its characteristic Raman band around 1600 cm^{-1}, assigned to aryl ring symmetric stretching vibration; while cellulose and hemicellulose bands overlap in the regions 800–1500 cm^{-1} as well as region 2800–3000 cm^{-1} [33]. Figure 2b reveals the Raman spectra of unloaded and metal-ions loaded SCL, while the assignment of the bands are presented in Table 1. As shown in the table, a number of bands were observed in the spectra of unloaded SCL. These include two moderate absorption peaks at 1605 and 1625 cm^{-1}, characteristic of ring conjugated C=C stretching vibration of lignin [34]. These particular peaks became very strong and prominent after the uptake of Ni^{2+}, Cr^{3+} and especially Co^{2+}, indicating that the lignin part of the lignocellulosic adsorbent play a vital role in the adsorption process. Change in intensities and/or peaks were also observed in other absorption bands, including those at the region of cellulose/hemicellulose overlap, suggesting the participation of all the major component of the biomass material in the uptake of the three metal ions.

3.1.2 SEM, EDAX and XRD analyses of SCL

Analysis surface morphology and elemental determination of SCL was carried out using Scanning Electron Microscope (JEOL JSM-6390 LV Model, Japan), coupled with Energy Dispersive Spectroscope. Figure 3a shows that the surface of the unloaded SCL was oval and irregularly shaped, revealing dispersed pores [19], which could possibly make the biomass a potential removal of toxic substances from polluted water [7]. The micrographs of metal-loaded SCL are shown in Figs 3(b-d). Although the oval shaped particles could still be noticed after the adsorption of Ni^{2+}, Cr^{3+} and Co^{2+} ions, nonetheless, the adsorption of the metal ions resulted in surface folding, indicating marked changes in the surface morphology of the adsorbent after metal loading.

Figure 4a shows the EDAX spectra of raw SCL [22]. Two dominant elements present in SCL, as revealed by EDAX, are carbon and oxygen, which constituted over 97% of the entire elemental composition. Nickel, chromium, and cobalt were not detected in the raw sample. However, after adsorption, about 3.52%, 4.56% and 6.57% nickel, chromium and cobalt were respectively detected in the sample loaded with the corresponding metal, thus confirming the interaction of SCL with the metal ions. The crystallinity of SCL was determined by X-ray diffractometry (XRD), using a Bruker BV 2D Phaser Benchtop X-ray diffraction (XRD) instrument with reflection geometry at 2θ values (10–90°) with a 5.240 s requisition time per step, operating with a Cu $K\alpha_1$ radiation source (λ = 0.15406 nm) at 50 kV and 30 mA. The XRD diffractograms of SCL (unloaded and metal-ion loaded) are depicted in Figure 4b. The XRD pattern of raw sample reveals one intense and prominent peak at around 2 theta 23° and other secondary peaks at around 2 theta 17°, 30° and 41°. The prominent and intense peak at around 2 theta 23° is characteristic of highly ordered crystalline cellulose [22]. Other non-prominent peaks indicate the presence

of a substantial amount of less ordered amorphous moieties such as lignin and polysaccharides in SCL [36]. After the uptake of Ni^{2+}, Cr^{3+} and Co^{2+} ions, the intensity of the prominent peak at around 2 theta 23° was observed to have decreased, while all other three secondary peaks appeared more pronounced, signifying the effects of metal ions uptake.

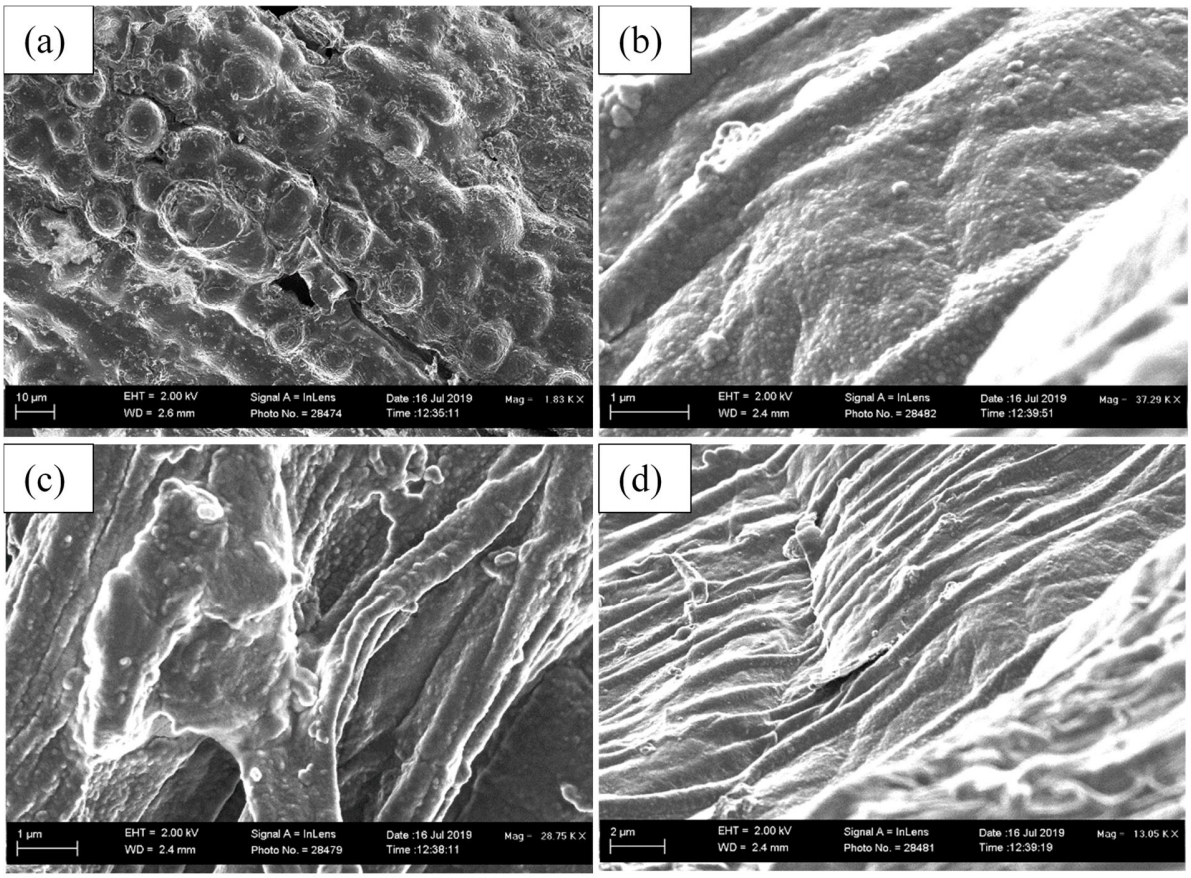

Fig. 3 SEM micrograms for adsorption of (a) unloaded (b) Ni-loaded (c) Cr-loaded and (d) Co-loaded SCL

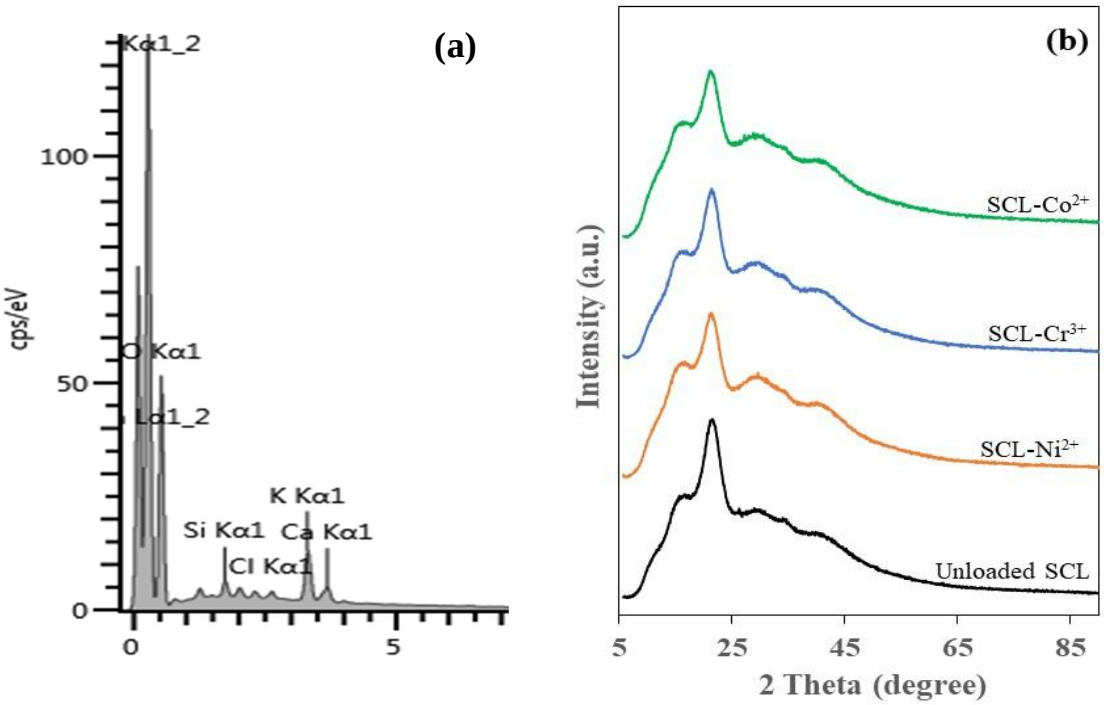

Fig. 4 EDAX [22] and XRD diffractograms of unloaded, Ni-loaded, Cr-loaded, and Co-loaded SCL

3.2 Metal-ions removal process

3.2.1 Effect of solution pH

Solution pH plays crucial role in the interaction of the adsorbates at the adsorbent surface [37]. Solution pH regulates adsorbate speciation, complexation, hydrolysis, solubility, precipitation, as well as density of charged species on the surface of an adsorbent during sorbate – sorbent interaction [38,39]. As shown in Figure 5a, solution pH greatly influenced the adsorption of Ni^{2+}, Cr^{3+} and Co^{2+} onto SCL. At 27 °C, optimum removal occurred at pH 4 for Cr^{3+} ions, and 5 for Ni^{2+} ions. Sorption increased with pH rise from 2 – 7 in the case of Co^{2+} ions. One possible explanation for these observations is the presence of high degree of protons at low pH. When an adsorptive solution is at very low pH, the binding sites on the adsorbent surface become protonated, thus rendering them unavailable for the cationic metal binding. With rise in pH, gradual deprotonation occurs at the surface, hence, more negatively charged ligands become available at the surface. The presence of negative charge density at the surface then promote electrostatic attraction between the cationic metal ion and the negatively charged species, leading to increasing cationic metal binding [40]. This is possibly responsible for the gradual ris e in % metal uptake observed as pH was increased from 2 – 4 for the sorption of Cr^{3+} ions, and 2 – 7 in the case of the removal of Ni^{2+} and Co^{2+} ions. The present investigation was limited to $pH \leq 7$ because of the difficulties in distinguishing real adsorption from precipitation of metal ions from solution at higher pH. For example, at $pH > 8$, Co(II) has been reported

to precipitate as $Co(OH)_2$ [41,42]. Therefore, in order to eliminate any possible interference as a result of precipitation, Ni^{2+} and Co^{2+} ions solutions were maintained at pH 6 for all subsequent studies. After the attainment of optimum, uptake of Cr^{3+} ions decreased. This, however, can be explained in terms of metal speciation. Cr(III), for example, appears as different species in aqueous solution – as hexa-aquachromium ($Cr(H_2O)_6^{3+}$) and its hydrolysis products [43], depending on the solution pH. It predominantly takes the form of Cr^{3+} at pH < 3; Cr^{3+} and $Cr(OH)^{2+}$ forms at around pH 4; $Cr(OH)^{2+}$ form at 4 ≤ pH ≥ 6, while $Cr(OH)_2^+$ results at pH > 6, together with precipitation as $Cr(OH)_3$ [43]. Hence, the highest % Cr^{3+} uptake at pH 4 probably indicates that Cr(III) was preferentially adsorbed on SCL as $Cr(H_2O)_6^{3+}$ and $Cr(OH)^{2+}$ species.

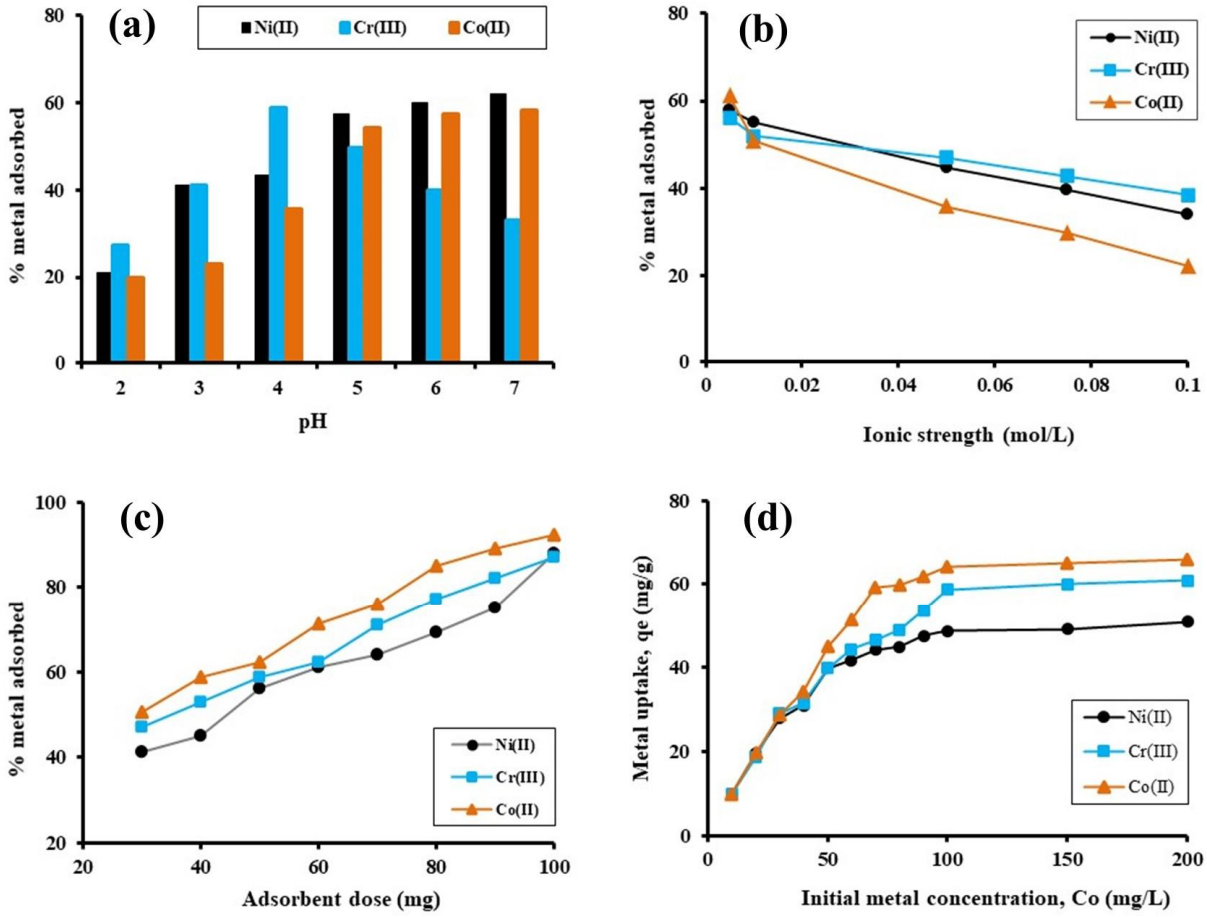

Fig. 5 Plots of effects of (a) pH (b) ionic strength (c) dose and (d) initial concentration on the adsorption of Ni^{2+}, Cr^{3+} and Co^{2+} ions onto SCL

3.2.2 Effect of ionic strength

The interactions between adsorbates and adsorbents at the surface of adsorbents are, in effect, partly regulated by the ionic strength of the solution. These interactions can be electrostatic and/or non-electrostatic in nature [44]. The effect of ionic strength on the adsorption of Ni^{2+}, Cr^{3+} and Co^{2+} ions onto SCL was investigated in the presence of NaCl as background electrolyte. As shown in Fig. 5b, metal ions removal decreased with increase in ionic strength of the solution. The effect was most pronounced on Co^{2+} adsorption: when the ionic strength was varied from 0.005 to 0.1 mol/L, percentage removal of Co^{2+} decreased by about 39%. Within the same concentration range, Ni^{2+} and Cr^{3+} removal dropped by 24% and 18%, respectively. Reports of many other investigations also showed decreasing metal ions uptake with improved ionic strength. For example, Cr adsorption was observed to decrease with increase in NaCl concentration, from 0 to 0.3 mol/L [45], while decrease in Ni(II) uptake was reported with enhancement of NaCl concentration from 0.0001 to 0.1 mol/L [46]. The reduction in metal ions uptake observed with increasing ionic strength could be attributed to possible growing competition between the metal ions and Na^{+} cations for the binding sites at the adsorbent surface [45-47]. Furthermore, the influence of electrostatic attraction might have also played a significant role: the enhancement of the concentration of NaCl in the solution possibly limited the accessibility of the metal ions to the adsorptive site at the SCL surface [47], consequently resulting in decreasing adherence of Ni^{2+}, Cr^{3+} and Co^{2+} ions to the adsorption sites on SCL surface.

3.2.3 Effect of solid to liquid ratio

A wise choice of solid (adsorbent) to liquid (adsorbate) ratio in any batch adsorption process goes a long way in determining the efficiency of the pollutant removal process. Hence the need to investigate the quantity of SCL needed to effectively remove Ni^{2+}, Cr^{3+} and Co^{2+} ions from aqueous medium at a fixed adsorbate (metal ions) concentration of 50 mg/L. Figure 5c illustrates the observed effects. SCL quantity in contact with 50 mL solution was varied from 30 – 100 mg. Under the chosen experimental condition, increase in metal ions uptake was observed with increase in adsorbent mass. For example, with 30 mg SCL in contact with the metal ions solution, around 41, 47 and 60 % Ni^{2+}, Cr^{3+} and Co^{2+} ions were respectively removed. The percent removal was, however, increases to around 88, 87 and 92% Ni^{2+}, Cr^{3+} and Co^{2+} ions, respectively with SCL mass of 100 mg. A similar observation was reported by Iqbala *et al*., in their report on the removal of Cd^{2+} and Pb^{2+} by mango peel waste [12]. The phenomenon is understandable in the sense that, at low adsorbent mass, fewer active sites were available for the binding of the metal ions. As the SCL mass increased, more active sites became exposed to the adsorbate [48], hence the steady increase in the percent metal removal observed.

3.2.4 Adsorption equilibrium process

Information about the isothermal behaviours of Ni^{2+}, Cr^{3+} and Co^{2+} ions adsorptions were obtained from the data generated from the study on the effect of initial concentrations of metal ions on the metal removal process. The experiment was performed at the concentrations of metal ions varying from 10 – 200 mg/L. As depicted in Figure 5d, increasing the initial concentrations of the metal ions exerted significant influence on the quantity of metal removed under the chosen experimental condition. General increase in metal uptake was observed with increasing the initial concentration of the respective metal ions from 10 – 100 mg/L. Adsorption–desorption equilibrium, however, appeared to have been attained at 100 mg/L initial concentration, after which further increase in concentration bore no significant influence on the metal removal by the chosen amount of SCL in the medium. Thus, the effect of varying the initial concentration on the metal removal process can be categorised into two stages – the pre-saturation and the saturation stages. The pre-saturation stage is the phenomenon observed by changing the initial metal ions concentration from 10 – 100 mg/L, while the observation between the initial concentration of 100 – 200 mg/L represents the saturation stage.

During the pre-saturation stage, there is the possibility of increase in collision rate between the metal ions and SCL due to increasing metal ion population in the bulk liquid phase. At low concentration, binding sites/metal ions ratio is large, leaving a few sites unoccupied. With increasing metal ions population, the gap narrowed, collision rate increased [49] and more active site became filled until none remained available for binding without changing the experimental condition. Moreover, there is the possibility of the removal of the restriction in the movement of the metal ions from the aqueous phase to the solid surface, which appeared to have occurred at low adsorbate concentration. The establishment of a high driving forces due to increasing metal ions population in the bulk solution phase must have allowed the removal of such initial barrier [50].

The saturation stage represents the point at which adsorption–desorption equilibrium became established. The near plateau observed at this stage signifies the negligible effect of further rise in the concentration of metal ions beyond 100 mg/L. At the beginning of the steady state, the amount of Ni^{2+}, Cr^{3+} and Co^{2+} ions removed were 48.8, 58.7 and 64.2 mg/g respectively, showing the order of removal efficiency of the three metal as $Co^{2+} > Cr^{3+} > Ni^{2+}$ ions. This corroborates the result of EDAX analysis which indicated that the adsorbent loaded with Co^{2+} had the highest metal composition, followed by that loaded with chromium and then nickel.

To determine the isotherm that best describes the adsorption of the three metals, data were fitted to the Langmuir, Freundlich, Temkin and Dubinin-Radushkevich (D-R) equilibrium models. Parameters were acquired from the linear plot of the respective models. Equations for the models have been stated in Equation 7 – 10. The suitability of a particular model was determined by the coefficient of determination,

R^2. Usually, R^2 measures the conformation of the regression line to the experimental data, and its values ranges from zero to one. A perfect fit is indicated by unity, although a value close to unity can be an indication of good fit. Values < 0.8 expresses the inadequacy of such a model in explaining the experimental data [45]. Table 2 lists the various parameters obtained from the models. The D-R model is considered inappropriate in explaining the isothermal behaviour, especially those of Ni^{2+} and Cr^{3+} ($R^2 < 8$). All the three other models showed good fits. Nevertheless, the Langmuir isotherm exhibited the best fit of all (R^2 of near unity), thus suggesting more of monolayer adsorption. This implied that the adsorption of Ni^{2+}, Cr^{3+} and Co^{2+} ions occurred at specific homogeneous sites and that the surface of SCL contained finite number of identical active sites [28,48]. The maximum monolayer adsorption, q_{max}, was determined to be 51.3, 62.5 and 66.7 mg/g for Ni^{2+}, Cr^{3+} and Co^{2+} ions respectively. This favourably compares with the performance of other adsorbents reported in the literatures for the removal of the three metal ions, Table 3.

The Freundlich model describes heterogeneous nature of a particular surface during adsorption process. The Freundlich constant *n* signifies the affinity of an adsorbate for an adsorbent. Its values were found around 3.0 for the adsorption of the three metal ions. The *n* values, being > 1, signify the favourability [51] and physical nature of the adsorption processes. The Dubinin-Radushkevich isotherm is often employed in distinguishing the nature of the process – whether physical or chemical [30]. In the present study, the values of the mean energy, E, expressed as $E = 1/\sqrt{2\beta}$, were found to be 5.00, 3.54 and 3.16 kJ/ mol for the adsorption of Ni^{2+}, Cr^{3+} and Co^{2+} ions, respectively. These values, being < 8, indicate that the metal removal processes were physical in nature [52].

Table 2 Comparison of the adsorption capacity of SCL with other previously used adsorbents

Adsorbent	**Temp./K**	**q_{max} (mg/g)**			**Reference**
		Ni^{2+}	*Cr^{3+}*	*Co^{2+}*	
Asplenium nidus L.	300	9.2	-	-	[53]
Oil palm calyxes	301	277.8	270.3	-	[7]
Activated Carbon from Hazelnut Shells	303	-	-	13.9	[42]
Moringa pods	293	5.5	3.2	-	[54]
Sargassum glaucescens nanoparticles	308	28.7	-	10.1	[55]
Xanthoceras Sorbifolia Bunge hull	N.S	187.96	-	126.1	[33]
Sugarcane leaf (SCL)	300	51.3	62.5	66.7	Current report

Table 3 Kinetic and equilibrium parameters for the adsorption of Ni^{2+}, Cr^{3+} and Co^{2+} onto SCL

Kinetic Model	*Parameter*	Ni^{2+}	Cr^{3+}	Co^{2+}
Pseudo-first order	R^2	0.9793	0.9624	0.9771
	k_1 (L/min)	0.0065	0.0093	0.0042
	q_e (mg/g)	41.2892	48.7156	59.0273
	$q_{e(calc)}$	22.64	18.88	23.52
Pseudo- second order	R^2	0.9827	0.9861	0.9624
	k_2 (g/mg min)	4.2E-5	2.5E-4	3.2E-4
	q_e (mg/g)	69.44	74.10	62.90
	$q_{e(calc)}$	67.54	72.90	61.5
Weber-Morris	R^2	0.9812	0.8584	0.9744
	k_α (mg/g $min^{½}$)	2.290	3.580	3.065
	C	19.866	7.167	8.766
Elovich	R^2	0.7387	0.8608	0.7934
	α	12.8744	3.4265	4.8050
	β	0.1086	0.0652	0.0869
Equilibrium isotherm model				
Langmuir	R^2	0.9984	0.9956	0.9885
	k_L (L/mg)	0.328	0.205	0.478
	q_{max} (mg/g)	51.282	62.500	66.667
Freundlich	R^2	0.9594	0.9306	0.9459
	k_F (L/mg)	21.900	20.578	24.028
	n	3.0865	3.0242	3.1792
Temkin	R^2	0.9667	0.9288	0.9258
	K_T (L/g)	1.39E-11	1.55E-10	6.35E-13
	b (kJ g/mol^2))	13.8030	20.3608	23.5302
Dubinin-Radushkevich (D-R)	R^2	0.7595	0.6648	0.8041
	q_m (mg/g)	40.246	43.676	51.573

3.2.4 Kinetics of the metal removal process

The optimum contact time for adsorption is an important parameter to be determined in the study of any adsorption process. A fast adsorption kinetics is an indication that a high efficiency of industrial wastewater remediation can be performed within a relatively short time. In the present study, the removal of Ni^{2+} and Cr^{3+} ions were relatively fast within the first 30 and 60 min, respectively (Figure 6a). After this first stage, metal uptake slowed and eventually approached equilibrium after 5 h. This observation is in agreement with a report by Azouaou *et al*. [48]. Meanwhile, the uptake of Co^{2+} ions was gradual from the beginning,

especially within the first 80 min. A minimal surge in uptake was observed between 80 and 180 min, after which the process slowed till 300 min where equilibrium appeared to have been attained. After a contact time of 6 h, about 62, 64 and 63 mg/g of Ni^{2+}, Cr^{3+} and Co^{2+} ions have been respectively removed. At the initial stage of the process, there was copious number of active sites available on the surface of SCL which were rapidly occupied by the metal ions, hence the sharp increase observed in metal uptake during the first stage. The slow stage observed later was due to depletion in sorption sites which eventually appeared to be completely filled after 120 min [12]. Therefore, a contact time of 120 min was chosen for subsequent studies.

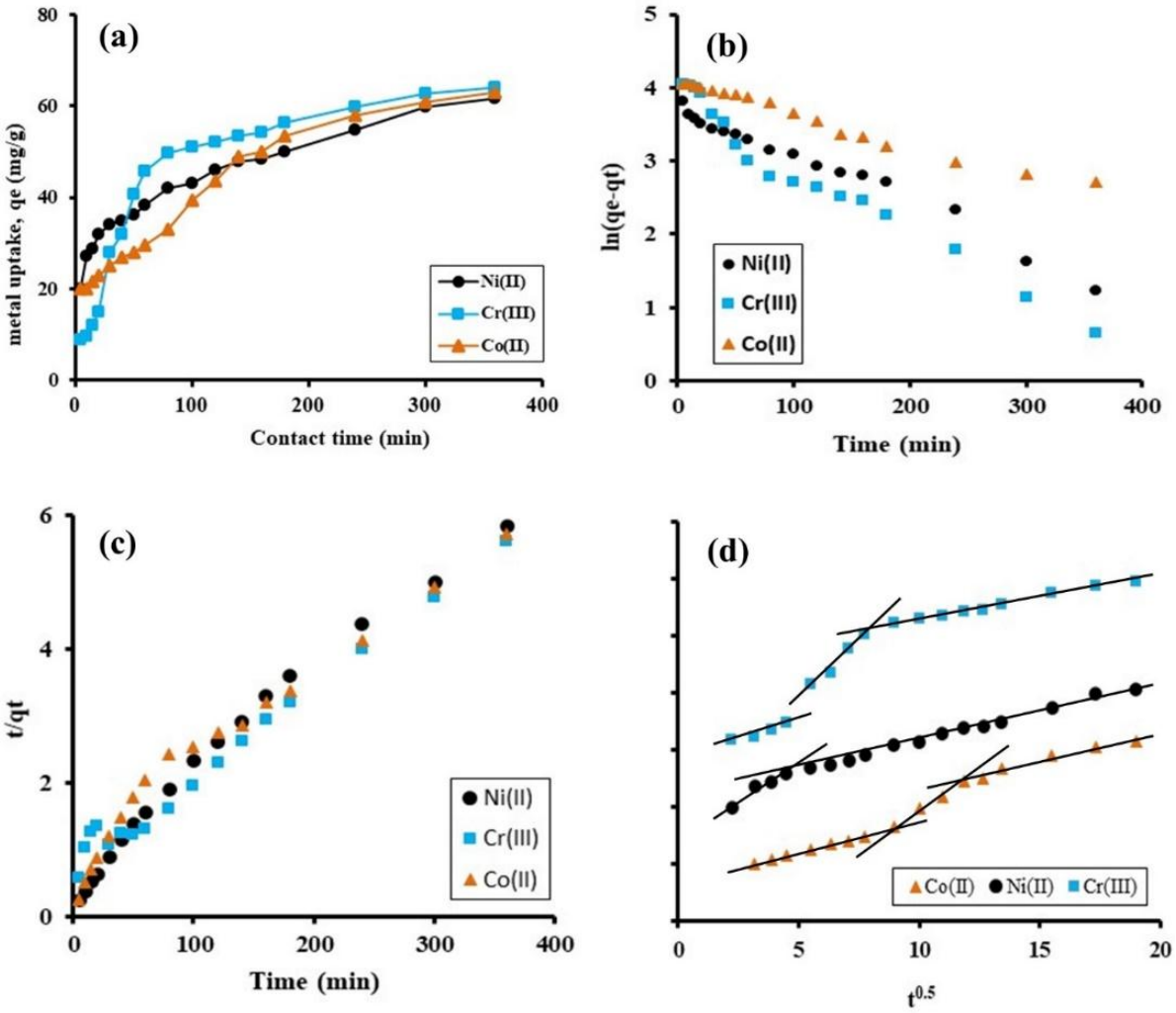

Fig. 6 Time dependent (a), Pseudo-first order (b), pseudo-second order (c) and Weber-Morris intraparticle plots for the adsorption of Ni2+, Cr3+ and Co2+ onto SCL

Kinetic modelling of the experimental data was performed to ascertain the best model or models that suitably explain the kinetics of the adsorption process; predict the rate limiting step and propose the mechanism of the adsorption processes. Models evaluated were the pseudo-first-order, pseudo-second order, Elovich and Weber-Morris. Like in the equilibrium study, the best model was selected based on the determination coefficient, R^2. As detailed in Table 2, it is only the Elovich model, among the kinetic models evaluated, that failed to describe the kinetic data – R^2 values were less than or around 0.8. Elovich model has been reported to be mainly valid for heterogeneous surfaces and the general applicability of the equation has been in chemisorption kinetics [56]. The failure of the model to describe the data suggests that the nature of SCL removal of Ni^{2+}, Cr^{3+} and Co^{2+} ions is physisorption. The other two kinetic models, though not perfect, demonstrated good fits of the experimental data. Figure 6(b,c) shows the kinetic plot for the pseudo-first and pseudo-second order models. A set of data that follows the pseudo-second order kinetics suggests the rate-limiting step of the adsorption process to be chemisorption. It thus predicts the involvement of valency forces through sharing or exchange of electron during adsorbate – adsorbent interaction [25]. That the adsorption of Ni^{2+}, Cr^{3+} and Co^{2+} ions demonstrated good fit when modelled with the pseudo-second-order is an indication of the involvement of a minimum of two steps, which most likely include metal or hydronium ion complex dissociation and binding of the metal ions with the surface active functional groups [20]. Although the pseudo-first order model demonstrated good fit of the experimental data, often times, the applicability of the model is limited to the earlier adsorption stage during which the adsorbate uptake increase with time is linear [57]. Moreover, the disparity between the experimental equilibrium uptake, $q_{e(exp)}$ and the calculated equilibrium uptake, $q_{e(calc)}$, for the pseudo-first-order, suggest that the pseudo-second-order kinetic model best explain the kinetic of the adsorption processes – for the pseudo-second-order model, the two values are very close to each other as shown in Table 2. A similar kinetic behaviour has been reported for the biosorption of Ni(II) and Pb(II) onto *Asplenium nidus* L [53].

The mechanism of the process was investigated by fitting data to the Weber-Morris model. The model reveals that the rate controlling step was not limited to the intra-particle diffusion. This is evident from the plot of quantity adsorbed, q_e (mg/g) against the square root of time, $t^{0.5}$ (Figure 6d) whose intercept failed to start from origin. The adsorption of Cr^{3+} and Co^{2+} ions occurred in three stages while that of Ni^{2+} ions involved two stages, predicting that the adsorption processes of the three metal ions were controlled by, at least, two of (i) external film diffusion (iii) surface diffusion (iii) intra-particle diffusion and (iv) adsorption elementary process [58,59]. The adsorption step has been known to be very fast [60], thus excluding it from possible rate limiting steps. On the other hand, the intercept, C, values obtained are large (19.9, 7.2 and 8.8 for Ni^{2+}, Cr^{3+} and Co^{2+} respectively), implicating the external film diffusion [57]. Hence, the rate limiting steps are possibly the external film diffusion and the intra-particle diffusion elementary steps. Findings from both isothermal and kinetic modelling all proposed physisorption process in the

removal of the three metal ions. Various characterization results also corroborated this submission. No new absorption peak was observed in the FTIR spectra after metal adsorption, while aside change in peak intensities, no other significant change was observed in XRD diffractograms of the samples. These reports suggest the exclusion of the formation of other compounds as a result of the interactions, thereby predicting the binding mechanism of Ni^{2+}, Cr^{3+} and Co^{2+} ions as physical, occurring mainly via van der Walls interaction [61]. On the other hand, the involvement of ion exchange mechanism cannot be ruled out. EDAX analysis revealed the presence of calcium and potassium on the SCL surface. The presence of these exchangeable cations and protons on the SCL surface were possibly exchanged with the heavy metal ions [62] during the removal of Ni^{2+}, Cr^{3+} and Co^{2+} ions. Therefore, the adsorption of the metal ions could be a complex process, involving physical as well as ion exchange-mechanism which the Dubinin–Radushkevich model could not adequately account for.

3.2.6 Thermodynamic studies

Thermodynamic parameters such as standard Gibb's free energy change, ΔG°, standard entropy change, ΔS° and standard enthalpy change, ΔH° of any adsorption process are often evaluated from the slope and intercept of a plot of vant's Hoff equation, represented by equation 11.

$$\ln K_c = \frac{\Delta S^o}{R} - \frac{\Delta H^o}{RT} \quad \ldots\ldots 11$$

Where K_c, the equilibrium constant for the adsorption process is expressed as

$$K_c = \frac{C_o - C_e}{C_o} \quad \ldots\ldots 12$$

R is the universal gas constant, given as 8.314 J /mol K, while T, represents temperature.

The thermodynamic parameters obtained for the sorption of Ni^{2+}, Cr^{3+} and Co^{2+} ions by SCL are presented in Table 4. The experiments, conducted at five different temperatures (293, 298, 303, 308 and 313 K), gave negative values for the standard Gibb's free energy change at all the temperatures studied. This implies that the adsorption of the three metal ions was feasible and spontaneous. Increase in the absolute values of ΔG° with rise in temperature suggests that the process will be more favoured by increasing temperature [7]. This was supported by the observation of rise in metal ions removal with increasing experimental temperature up to the highest temperature studied. The standard enthalpy change, ΔH° for the three processes was observed to be positive, implying that the process was endothermic, corroborating the information obtained from ΔG°. This means that external forces (energy) may be required

in driving the adsorption processes. The magnitude of ΔH° for the adsorption of the three metal ions were obtained as 8.76, 7.59 and 6.16 kJ/mol for Ni^{2+}, Cr^{3+} and Co^{2+} ions. These values, ranging from 4 to around 8 kJ/mol, propose the processes to be physisorption [63]. The standard entropy change, ΔS° values were observed to be negative, implying that the sorption of Ni^{2+}, Cr^{3+} and Co^{2+} ions occurred with decrease in disorderliness or randomness at the interface between solid and liquid [64].

Table 4 Thermodynamic parameters for the adsorption of Ni^{2+}, Cr^{3+} and Co^{2+} onto SCL

Metal ion	**Parameter**							
	ΔH°	**ΔS°**	**ΔG°**					
	(kJ/mol)	***(J/K mol)***	***(kJ/mol)***					
			293 K	**298 K**	**303 K**	**308 K**	**313 K**	**318 K**
Ni^{2+}	8.760	-31.604	-493.8	-643.6	-800.7	-1019.0	-1173.6	-1238.3
Cr^{3+}	7.587	-27.614	-560.5	-648.9	-737.2	-826.5	-1044.3	-1271.9
Co^{2+}	6.157	-21.868	-263.3	-367.9	-434.4	-585.0	-680.3	-811.15

4 Conclusion

The adsorptive capacity of SCL, a biomass of waste sugarcane leaves, has been tested on three toxic heavy metal ions, Ni^{2+}, Cr^{3+} and Co^{2+} ions. Characterization by FTIR, Raman, SEM, EDAX and XRD suggest that the SCL possesses the qualities of a good adsorbent for the removal of pollutants from aqueous medium. Investigation of the effects of various parameters known to influence adsorption reveals that, under the chosen experimental condition, Cr^{3+} best adsorbed at pH 4 as $Cr(H_2O)_6^{3+}$ and $Cr(OH)^{2+}$ species, while uptake of Ni^{2+} and Co^{2+} ions increased with rise in solution pH from 2 – 7 (the highest investigated). Metal uptake decreased with enhanced ionic strength and increase in percent metal removal was observed with increase in the amount of SCL in the solution. Initial sharp uptake was noticed at the initial stage, which later slowed with increase in SCL-metal ions contact time. Equilibrium metal ions concentration was attained after 100 mg/L initial adsorbate concentration for the three metal ions. Kinetic and isothermal modelling propose physisorption process in the removal of the three metal ions. The models also suggest monolayer adsorption and, at least, one other stage, apart from intraparticle diffusion, in the rate controlling steps in the mechanism of the process. Thermodynamic study submits that the sorption processes is spontaneous and feasible, endothermic and occurred with increase in the randomness of the adsorption system as the SCL adsorbed the metal ions, indicating that the SCL, if properly harnessed, has the potential of the removal of toxic Ni^{2+}, Cr^{3+} and Co^{2+} ions from polluted water.

5 Authors' contributions

Oludoyin Adeseun Adigun: Experimental, data analyses, preparation of initial draft and manuscript's revision; Vincent Olukayode Oninla: Data validation and analyses, manuscript's editing and revision; Kabir Oyedokun and Ncholu Manyala: Characterization and manuscript's editing; N. A. Adesola Babarinde: Conceptualization, supervision and manuscript's editing. All authors approved the final manuscript before submission.

Acknowledgements: The authors acknowledge the Wood Extraction Laboratory of Chemistry Department, University of Ibadan; Central Research Laboratory, University of Ibadan; Polymer & Biophysical Chemistry Research Laboratory, Obafemi Awolowo University, Ile-Ife, Nigeria; and the Institute of Applied Materials, Carbon Technology and Materials, University of Pretoria, South Africa, for permission to access their research facilities.

Conflicts of Interest: The authors declare no conflict of interest.

References

1. Wang, Q. Urbanization and global health: The role of air pollution. *Iran J Public Health* 2018, *47*, 1644-1652.
2. Azimi, A.; Azari, A.; Rezakazemi, M.; Ansarpour, M. Removal of heavy metals from industrial wastewaters: A review. *ChemBioEng Reviews* 2017, *4*, 37-59, doi:10.1002/cben.201600010.
3. Aljeboree, A.M.; Alshirifi, A.N.; Alkaim, A.F. Kinetics and equilibrium study for the adsorption of textile dyes on coconut shell activated carbon. *Arabian Journal of Chemistry* 2017, *10*, S3381-S3393, doi:https://doi.org/10.1016/j.arabjc.2014.01.020.
4. Jannat Abadi, M.H.; Nouri, S.M.M.; Zhiani, R.; Heydarzadeh, H.D.; Motavalizadehkakhky, A. Removal of tetracycline from aqueous solution using Fe-doped zeolite. *International Journal of Industrial Chemistry* 2019, *10*, 291-300, doi:10.1007/s40090-019-0191-6.
5. Naushad, M.; Ahamad, T.; Sharma, G.; Al-Muhtaseb, A.a.H.; Albadarin, A.B.; Alam, M.M.; Alothman, Z.A.; Alshehri, S.M.; Ghfar, A.A. Synthesis and characterization of a new starch/SnO2 nanocomposite for efficient adsorption of toxic Hg2+ metal ion. *Chemical Engineering Journal* 2016, *300*, 306-316, doi:https://doi.org/10.1016/j.cej.2016.04.084.
6. Bem, E.M.; Orlowski, C.; Piotrowski, J.K.; Januszewski, K.; Pajak, J. Cadmium, zinc, copper, and metallothionein levels in the kidney and liver of inhabitants of Upper Silesia (Poland). *International Archives of Occupational and Environmental Health* 1993, *65*, 57-63, doi:10.1007/BF00586060.
7. Oninla, V.O.; Olatunde, A.M.; Babalola, J.O.; Adesanmi, O.J.; Towolawi, G.S.; Awokoya, K.N. Qualitative assessments of the biomass from oil palm calyxes and its application in heavy metals removal from polluted water. *Journal of Environmental Chemical Engineering* 2018, *6*, 4044-4053, doi:10.1016/j.jece.2018.05.030.

8. Bazrafshan, E.; Mohammadi, L.; Ansari-Moghaddam, A.; Mahvi, A.H. Heavy metals removal from aqueous environments by electrocoagulation process– a systematic review. *Journal of Environmental Health Science and Engineering* 2015, *13*, 74, doi:10.1186/s40201-015-0233-8.
9. Fu, F.; Wang, Q. Removal of heavy metal ions from wastewaters: A review. *Journal of Environmental Management* 2011, *92*, 407-418, doi:https://doi.org/10.1016/j.jenvman.2010.11.011.
10. McKew, B.A.; Dumbrell, A.J.; Taylor, J.D.; McGenity, T.J.; Underwood, G.J.C. Differences between aerobic and anaerobic degradation of microphytobenthic biofilm-derived organic matter within intertidal sediments. *FEMS Microbiology Ecology* 2013, *84*, 495-509, doi:10.1111/1574-6941.12077.
11. Wang, L.; Wang, Y.; Ma, F.; Tankpa, V.; Bai, S.; Guo, X.; Wang, X. Mechanisms and reutilization of modified biochar used for removal of heavy metals from wastewater: A review. *Science of The Total Environment* 2019, *668*, 1298-1309, doi:https://doi.org/10.1016/j.scitotenv.2019.03.011.
12. Iqbal, M.; Saeed, A.; Zafar, S.I. FTIR spectrophotometry, kinetics and adsorption isotherms modeling, ion exchange, and EDX analysis for understanding the mechanism of Cd2+ and Pb2+ removal by mango peel waste. *Journal of Hazardous Materials* 2009, *164*, 161-171, doi:https://doi.org/10.1016/j.jhazmat.2008.07.141.
13. Kyzas, G.Z.; Kostoglou, M. Green adsorbents for wastewaters: A critical review. *Materials* 2014, *7*, 333-364.
14. Chen, Z.; Zhang, S.; Liu, Y.; Alharbi, N.S.; Rabah, S.O.; Wang, S.; Wang, X. Synthesis and fabrication of g-C3N4-based materials and their application in elimination of pollutants. *Science of The Total Environment* 2020, *731*, 139054, doi:https://doi.org/10.1016/j.scitotenv.2020.139054.
15. WANG, X.; LI, X.; WANG, J.; ZHU, H. Recent advances in carbon nitride-based nanomaterials for the removal of heavy metal ions from aqueous solution. *Journal of Inorganic Materials* 2020, *35*, 260-270.
16. WANG, X.-X.; YU, S.-J.; WANG, X.-K. Removal of radionuclides by metal-organic framework-based materials. *Journal of Inorganic Materials* 2019, *34* 17–26.
17. Sari, A.; Tuzen, M. Kinetic and equilibrium studies of biosorption of Pb(II) and Cd(II) from aqueous solution by macrofungus (Amanita rubescens) biomass. *J Hazard Mater* 2009, *164*, 1004-1011, doi:10.1016/j.jhazmat.2008.09.002.
18. Mohammod, M.; Sen, T.K.; Maitra, S.; Dutta, B.K. Removal of Zn2+ from aqueous solution using castor seed hull. *Water, Air, & Soil Pollution* 2011, *215*, 609-620, doi:10.1007/s11270-010-0503-0.
19. Oh, G.H.; Park, C.R. Preparation and characteristics of rice-straw-based porous carbons with high adsorption capacity. *Fuel* 2002, *81*, 327-336, doi:https://doi.org/10.1016/S0016-2361(01)00171-5.
20. Castro, L.; Blázquez, M.L.; González, F.; Muñoz, J.A.; Ballester, A. Biosorption of Zn(II) from industrial effluents using sugar beet pulp and F. vesiculosus: From laboratory tests to a pilot approach. *The Science of the total environment* 2017, *598*, 856-866, doi:10.1016/j.scitotenv.2017.04.138.
21. Kim, Y.H.; Yeon Park, J.; Yoo, Y.J.; Kwak, J.W. Removal of lead using xanthated marine brown alga, Undaria pinnatifida. *Process Biochemistry* 1999, *34*, 647-652, doi:https://doi.org/10.1016/S0032-9592(98)00137-X.
22. Adigun, O.A.; Oninla, V.O.; Babarinde, N.A.A. Application of sugarcane leaves as biomass in the removal of cadmium(II), lead(II) and zinc(II) ions from polluted water. *International Journal of Energy and Water Resources* 2019, *3*, 141-152, doi:10.1007/s42108-019-00024-w.
23. Mathew, B.B.; Jaishankar, M.; Biju, V.G.; Krishnamurthy Nideghatta, B. Role of bioadsorbents in reducing toxic metals. *J Toxicol* 2016, *2016*, 4369604-4369604, doi:10.1155/2016/4369604.

24. Simonin, J.-P. On the comparison of pseudo-first order and pseudo-second order rate laws in the modeling of adsorption kinetics. *Chemical Engineering Journal* 2016, *300*, 254-263, doi:https://doi.org/10.1016/j.cej.2016.04.079.
25. Ho, Y.S.; McKay, G. Pseudo-second order model for sorption processes. *Process Biochemistry* 1999, *34*, 451-465, doi:https://doi.org/10.1016/S0032-9592(98)00112-5.
26. Ayawei, N.; Ebelegi, A.N.; Wankasi, D. Modelling and interpretation of adsorption isotherms. *Journal of Chemistry* 2017, *2017*, 3039817, doi:10.1155/2017/3039817.
27. Campos, N.; Barbosa, C.; Rodríguez-Díaz, J.; Duarte, M. Removal of naphthenic acids using activated charcoal: Kinetic and equilibrium studies. *Adsorption Science & Technology* 2018, *36*, 026361741877384, doi:10.1177/0263617418773844.
28. Langmuir, I. The adsorption of gases on plane surfaces of glass, mica and platinum. *Journal of the American Chemical Society* 1918, *40*, 1361-1403, doi:10.1021/ja02242a004.
29. Ng, C.; Losso, J.N.; Marshall, W.E.; Rao, R.M. Freundlich adsorption isotherms of agricultural by-product-based powdered activated carbons in a geosmin–water system. *Bioresource Technology* 2002, *85*, 131-135, doi:https://doi.org/10.1016/S0960-8524(02)00093-7.
30. Dada, A.O.; Olalekan, A.; Olatunya, A.; Dada, O. Langmuir, Freundlich, Temkin and Dubinin–Radushkevich isotherms studies of equilibrium sorption of Zn 2+ unto phosphoric acid modified rice husk. *J. Appl. Chem.* 2012, *3*, 38-45, doi:10.9790/5736-0313845.
31. Sasmal, S.; Goud, V.V.; Mohanty, K. Characterization of biomasses available in the region of North-East India for production of biofuels. *Biomass and Bioenergy* 2012, *45*, 212-220, doi:https://doi.org/10.1016/j.biombioe.2012.06.008.
32. Agarwal, U.P.; McSweeny, J.D.; Ralph, S.A. FT–Raman investigation of milled-Wood lignins: Softwood, hardwood, and chemically modified black spruce lignins. *Journal of Wood Chemistry and Technology* 2011, *31*, 324-344, doi:10.1080/02773813.2011.562338.
33. Zhang, X.; Chen, S.; Ramaswamy, S.; Kim, Y.S.; Xu, F. Obtaining pure spectra of hemicellulose and cellulose from poplar cell wall Raman imaging data. *Cellulose* 2017, *24*, 4671-4682, doi:10.1007/s10570-017-1486-4.
34. Gierlinger, N.; Schwanninger, M. Chemical imaging of poplar wood cell walls by confocal raman microscopy. *Plant Physiology* 2006, *140*, 1246-1254, doi:10.1104/pp.105.066993.
35. Soliman, M. Advanced nanoscale characterization of plants and plant-derived materials for sustainable agriculture and renewable energy. Electronic Theses and Dissertations, https://stars.library.ucf.edu/etd/6221. , 2018.
36. Reddy, D.H.K.; Seshaiah, K.; Reddy, A.V.R.; Rao, M.M.; Wang, M.C. Biosorption of Pb2+ from aqueous solutions by Moringa oleifera bark: Equilibrium and kinetic studies. *Journal of Hazardous Materials* 2010, *174*, 831-838, doi:https://doi.org/10.1016/j.jhazmat.2009.09.128.
37. Vijayaraghavan, K.; Rangabhashiyam, S.; Ashokkumar, T.; Arockiaraj, J. Assessment of samarium biosorption from aqueous solution by brown macroalga Turbinaria conoides. *Journal of the Taiwan Institute of Chemical Engineers* 2017, *74*, 113-120, doi:https://doi.org/10.1016/j.jtice.2017.02.003.
38. Kushwaha, A.K.; Gupta, N.; Chattopadhyaya, M.C. Adsorption behavior of lead onto a new class of functionalized silica gel. *Arabian Journal of Chemistry* 2017, *10*, S81-S89, doi:https://doi.org/10.1016/j.arabjc.2012.06.010.
39. Koretsky, C. The significance of surface complexation reactions in hydrologic systems: A geochemist's perspective. *Journal of Hydrology - J HYDROL* 2000, *230*, doi:10.1016/S0022-1694(00)00215-8.
40. Babarinde, A.; Babalola, J.O.; Adegoke, J.; Osundeko, A.O.; Olasehinde, S.; Omodehin, A.; Nurhe, E. Biosorption of Ni(II), Cr(III), and Co(II) from solutions using Acalypha hispida leaf: Kinetics,

equilibrium, and thermodynamics. *Journal of Chemistry* 2013, *2013*, 460635, doi:10.1155/2013/460635.
41. Bernabé, I.; Gómez, J.M.; Díez, E.; Sáez, P.; Rodríguez, A. Optimization and adsorption-based recovery of cobalt using activated disordered mesoporous carbons. *Advances in Materials Science and Engineering* 2019, *2019*, 3430176, doi:10.1155/2019/3430176.
42. Demirbaş, E. Adsorption of cobalt(II) ions from aqueous solution onto activated carbon prepared from hazelnut hells. *Adsorption Science & Technology* 2003, *21*, 951-963, doi:10.1260/02636170360744380.
43. Alemu, A.; Lemma, B.; Gabbiye, N. Adsorption of chromium (III) from aqueous solution using vesicular basalt rock. *Cogent Environmental Science* 2019, *5*, doi:10.1080/23311843.2019.1650416.
44. El Ass, k. Adsorption of cadmium and copper onto natural clay: isotherm, kinetic and thermodynamic studies. *Global NEST Journal* 2018, *20*, 198-207.
45. Zhang, D.; Ma, Y.; Feng, H.; Hao, Y. Adsorption of Cr(VI) from aqueous solution using catbon-microsilica composite adsorbent. *Journal of the Chilean Chemical Society* 2012, *57*, 964-968.
46. Musso, T.B.; Parolo, M.E.; Pettinari, G. pH, ionic strength, and ion competition effect on Cu(II) and Ni(II) sorption by a Na-bentonite used as liner material. *Polish Journal of Environmental Studies* 2019, *28*, 2299-2309, doi:10.15244/pjoes/84922.
47. Larous, S.; Meniai, A.H.; Lehocine, M.B. Experimental study of the removal of copper from aqueous solutions by adsorption using sawdust. *Desalination* 2005, *185*, 483-490, doi:https://doi.org/10.1016/j.desal.2005.03.090.
48. Azouaou, N.; Sadaoui, Z.; Djaafri, A.; Mokaddem, H. Adsorption of cadmium from aqueous solution onto untreated coffee grounds: equilibrium, kinetics and thermodynamics. *J Hazard Mater* 2010, *184*, 126-134, doi:10.1016/j.jhazmat.2010.08.014.
49. Rashid, R.A.; Jawad, A.H.; Ishak, M.A.M.; Kasim, N.N. KOH-activated carbon developed from biomass waste: adsorption equilibrium, kinetic and thermodynamic studies for Methylene blue uptake. *Desalination and Water Treatment* 2016, *57*, 27226-27236, doi:10.1080/19443994.2016.1167630.
50. Senthil Kumar, P.; Senthamarai, C.; Durgadevi, A. Adsorption kinetics, mechanism, isotherm, and thermodynamic analysis of copper ions onto the surface modified agricultural waste. *Environmental Progress & Sustainable Energy* 2014, *33*, 28-37, doi:10.1002/ep.11741.
51. Liu, X.; Chen, Z.Q.; Han, B.; Su, C.L.; Han, Q.; Chen, W.Z. Biosorption of copper ions from aqueous solution using rape straw powders: Optimization, equilibrium and kinetic studies. *Ecotoxicology and environmental safety* 2018, *150*, 251-259, doi:10.1016/j.ecoenv.2017.12.042.
52. Wang, G.; Chang, Q.; Zhang, M.; Han, X. Effect of pH on the removal of Cr(III) and Cr(VI) from aqueous solution by modified polyethyleneimine. *Reactive and Functional Polymers* 2013, *73*, 1439–1446, doi:10.1016/j.reactfunctpolym.2013.07.009.
53. Dissanayake, D.M.R.E.A.; Wijesinghe, W.M.K.E.H.; Iqbal, S.S.; Priyantha, N.; Iqbal, M.C.M. Isotherm and kinetic study on Ni(II) and Pb(II) biosorption by the fern Asplenium nidus L. *Ecological Engineering* 2016, *88*, 237-241, doi:https://doi.org/10.1016/j.ecoleng.2015.12.028.
54. Matouq, M.; Jildeh, N.; Qtaishat, M.; Hindiyeh, M.; Al Syouf, M.Q. The adsorption kinetics and modeling for heavy metals removal from wastewater by Moringa pods. *Journal of Environmental Chemical Engineering* 2015, *3*, 775-784, doi:https://doi.org/10.1016/j.jece.2015.03.027.
55. Esmaeili, A.; Aghababai Beni, A. Biosorption of nickel and cobalt from plant effluent by Sargassum glaucescens nanoparticles at new membrane reactor. *International Journal of Environmental Science and Technology* 2015, *12*, doi:10.1007/s13762-014-0744-3.

56. Cheung, C.W.; Porter, J.F.; McKay, G. Elovich equation and modified second-order equation for sorption of cadmium ions onto bone char. *Journal of Chemical Technology & Biotechnology* 2000, *75*, 963-970, doi:10.1002/1097-4660(200011)75:11<963::aid-jctb302>3.0.co;2-z.
57. Thitame, P.V. Adsorptive removal of reactive dyes from aqueous solution using activated carbon synthesized from waste biomass materials. *International journal of environmental science and technology* 2016, *v. 13*, pp. 561-570-2016 v.2013 no.2012, doi:10.1007/s13762-015-0901-3.
58. Can, M. Studies of the kinetics for rhodium adsorption onto gallic acid derived polymer: the application of nonlinear regression analysis. *Acta Physica Polonica Series a* 2015, *127*, 1308-1310, doi:10.12693/APhysPolA.127.1308.
59. Suganya, S.; Senthil Kumar, P. Influence of ultrasonic waves on preparation of active carbon from coffee waste for the reclamation of effluents containing Cr(VI) ions. *Journal of Industrial and Engineering Chemistry* 2018, *60*, 418-430, doi:https://doi.org/10.1016/j.jiec.2017.11.029.
60. Albadarin, A.B.; Mangwandi, C.; Al-Muhtaseb, A.a.H.; Walker, G.M.; Allen, S.J.; Ahmad, M.N.M. Kinetic and thermodynamics of chromium ions adsorption onto low-cost dolomite adsorbent. *Chemical Engineering Journal* 2012, *179*, 193-202, doi:https://doi.org/10.1016/j.cej.2011.10.080.
61. Lozovski, V.; Khudik, B. The new mechanism of physical adsorption on solid surface. II. Adsorption of polar molecules. *Physica Status Solidi B-basic Solid State Physics - PHYS STATUS SOLIDI B-BASIC SO* 1990, *160*, 137-142, doi:10.1002/pssb.2221600110.
62. Dávila-Guzmán, N.E.; de Jesús Cerino-Córdova, F.; Soto-Regalado, E.; Rangel-Mendez, J.R.; Díaz-Flores, P.E.; Garza-Gonzalez, M.T.; Loredo-Medrano, J.A. Copper biosorption by spent coffee ground: Equilibrium, kinetics, and mechanism. *CLEAN – Soil, Air, Water* 2013, *41*, 557-564, doi:10.1002/clen.201200109.
63. Sims, R.A.; Harmer, S.L.; Quinton, J.S. The role of physisorption and chemisorption in the oscillatory adsorption of organosilanes on aluminium oxide. *Polymers (Basel)* 2019, *11*, 410, doi:10.3390/polym11030410.
64. Nithya, K.; Sathish, A.; Kumar, P.S.; Ramachandran, T. Functional group-assisted green synthesised superparamagnetic nanoparticles for the rapid removal of hexavalent chromium from aqueous solution. In *IET Nanobiotechnology*, Institution of Engineering and Technology: 2017; Vol. 11, pp 852-860.